Published in final edited form as:
Nature. 2013 January 10; 493(7431): 231–235. doi:10.1038/nature11661.

Control of somatic tissue differentiation by the long non-coding RNA TINCR

Markus Kretz[1], **Zurab Siprashvili**[1,*], **Ci Chu**[1,*], **Dan E. Webster**[1,*], **Ashley Zehnder**[1], **Kun Qu**[1], **Carolyn S. Lee**[1], **Ross J. Flockhart**[1], **Abigail F. Groff**[1], **Jennifer Chow**[1], **Danielle Johnston**[1], **Grace E. Kim**[1], **Robert C. Spitale**[1], **Ryan A. Flynn**[1], **Grace X. Y. Zheng**[1], **Subhadra Aiyer**[2], **Arjun Raj**[2], **John L. Rinn**[3], **Howard Y. Chang**[1,4], and **Paul A. Khavari**[1,5]

[1]The Program in Epithelial Biology, Stanford University School of Medicine, Stanford, California 94305, USA

[2]Department of Bioengineering, University of Pennsylvania, Philadelphia, Pennsylvania 19104, USA

[3]Department of Stem Cell and Regenerative Biology, Harvard University, Cambridge, Massachusetts 02138, USA

[4]Howard Hughes Medical Institute, Stanford, California 94305, USA

[5]Veterans Affairs Palo Alto Healthcare System, Palo Alto, California 94304, USA

Abstract

Several of the thousands of human long non-coding RNAs (lncRNAs) have been functionally characterized[1–4]; however, potential roles for lncRNAs in somatic tissue differentiation remain poorly understood. Here we show that a 3.7-kilobase lncRNA, terminal differentiation-induced ncRNA (TINCR), controls human epidermal differentiation by a post-transcriptional mechanism. TINCR is required for high messenger RNA abundance of key differentiation genes, many of which are mutated in human skin diseases, including *FLG, LOR, ALOXE3, ALOX12B, ABCA12, CASP14* and *ELOVL3*. TINCR-deficient epidermis lacked terminal differentiation ultrastructure, including keratohyalin granules and intact lamellar bodies. Genome-scale RNA interactome analysis revealed that TINCR interacts with a range of differentiation mRNAs. TINCR–mRNA interaction occurs through a 25-nucleotide ‘TINCR box’ motif that is strongly enriched in interacting mRNAs and required for TINCR binding. A high-throughput screen to analyse TINCR binding capacity to approximately 9,400 human recombinant proteins revealed direct binding of *TINCR* RNA to the staufen1 (STAU1) protein. STAU1-deficient tissue

Correspondence and requests for materials should be addressed to H.Y.C. (howchang@stanford.edu) or P.A.K. (khavari@stanford.edu).
*These authors contributed equally to this work.

Full Methods and any associated references are available in the online version of the paper.

Supplementary Information is available in the online version of the paper.

Author Contributions M.K. designed and executed experiments, analysed data and wrote the manuscript. D.E.W., Z.S., C.C., A.Z., C.S.L., R.J.F., K.Q., J.C., D.J., G.X.Y.Z., G.E.K., A.F.G., R.C.S., R.A.F. and S.A. executed experiments, analysed data and contributed to design of experimentation. A.R. and J.L.R. helped design experiments and analysed data. P.A.K. and H.Y.C. designed experiments, analysed data and wrote the manuscript.

Sequence and array data are deposited in the Gene Expression Omnibus database under the accession number GSE35468.

The authors declare no competing financial interests.

Readers are welcome to comment on the online version of the paper.

recapitulated the impaired differentiation seen with TINCR depletion. Loss of *UPF1* and *UPF2*, both of which are required for STAU1-mediated RNA decay, however, did not have differentiation effects. Instead, the TINCR–STAU1 complex seems to mediate stabilization of differentiation mRNAs, such as *KRT80*. These data identify TINCR as a key lncRNA required for somatic tissue differentiation, which occurs through lncRNA binding to differentiation mRNAs to ensure their expression.

LncRNAs regulate a variety of processes[1–3,5], yet their effects on homeostasis in somatic tissues such as epidermis are not fully defined. Transcriptome sequencing of progenitor and differentiating human keratinocytes was undertaken using the Illumina paired-end HiSeq platform with a read length of 101 nucleotides at about 110 million mapped reads per sample, with consistency verified by quantitative reverse transciptase PCR (qRT–PCR) (Supplementary Fig. 1a–c). TINCR, an uncharacterized lncRNA[6], was among the most highly induced lncRNAs of the 258 annotated non-coding RNAs changing during differentiation (Fig. 1a and Supplementary Table 1). The *TINCR* gene resides on chromosome 19 in humans between the *SAFB2* and *ZNRF4* genes (Fig. 1b), a locus conserved with a syntenic non-coding region on mouse chromosome 17qD. *TINCR* produces a 3.7-kilobase (kb) transcript induced >150-fold during epidermal differentiation (Fig. 1c–e). *TINCR* is downregulated in human squamous cell carcinoma specimens, consistent with decreased differentiation seen in squamous cell carcinomas (Supplementary Fig. 1d). Single-molecule RNA fluorescence *in situ* hybridization (FISH) identified 80.6% of TINCR molecules newly acquired during differentiation within the cytoplasm (Supplementary Fig. 1e, f). FISH in human epidermis showed enrichment of TINCR in differentiated layers (Supplementary Fig. 1g). TINCR is therefore a differentiation-induced, predominantly cytoplasmic lncRNA.

TINCR function was assessed by RNA interference in organotypic human epidermal tissue, a setting that recapitulates the structure and gene expression of human epidermis[7,8]. Although TINCR-deficient epidermis stratified normally, the expression of key differentiation genes mutated in human diseases of abnormal epidermal function[9–11] was markedly reduced at the protein (Fig. 2a) and mRNA (Fig. 2b) levels. TINCR is thus required for normal induction of key protein mediators of epidermal differentiation.

Transcript profiling of TINCR-depleted epidermis demonstrated that TINCR loss disrupted the expression of 394 genes (Supplementary Fig. 2a and Supplementary Table 2). TINCR-regulated genes were enriched for differentiation-associated epidermal barrier formation-related Gene Ontology (GO) terms (Fig. 2c). Barrier formation requires genes encoding the protein structure of the terminally differentiated stratum corneum, such as loricrin and filaggrin, as well as those synthesizing specific water-impermeable lipids[12]. GO terms related to the latter were enriched in genes altered by TINCR loss, as were the mRNA levels of genes in this subset that are genetically non-redundant for epidermal barrier formation[13–15] (Fig. 2d). Furthermore, caspase 14, implicated in proteolysis needed for epidermal barrier function[16], was diminished by 83.7% with TINCR loss. Protein and lipid barrier ultrastructures involved in barrier formation were abnormal in the outer layers of TINCR-deficient epidermis, including protein-rich keratohyalin granules (Fig. 2e) and the lipid-rich lamellar bodies (Fig. 2f). Deficiencies in these structures are characteristic of human genodermatoses with abnormal skin barrier function, including ichthyosis vulgaris and harlequin ichthyosis. No regions of normal keratohyalin granule formation were observed in TINCR-deficient epidermis, and the number of lamellar bodies in the stratum granulosum of TINCR-deficient human epidermal tissue was reduced by 81.4%. TINCR is thus required for the induction of genes that form the cellular structures that mediate differentiation-associated epidermal barrier formation.

To determine the mechanisms of TINCR action, we developed two assays to analyse the *TINCR* RNA and protein interactome (Supplementary Fig. 2d). Given its cytoplasmic location (Supplementary Fig. 1e), TINCR control of epidermal barrier genes may occur at the post-transcriptional level through direct association with target mRNAs. To test this, we developed RNA interactome analysis, followed by deep sequencing (RIA-Seq) (Supplementary Fig. 2d, left). Thirty-eight biotinylated DNA probes (Supplementary Table 3) were designed in even- and odd-numbered pools (Supplementary Fig. 2e). These two pools were used separately in a multiplex fashion for pull-down of endogenous TINCR and associated RNAs in differentiated keratinocytes (Supplementary Fig. 2d, left), similar to recent approaches to single-molecule RNA FISH[17] and chromatin isolation by RNA purification[18]. To discover transcripts enriched by TINCR pull-down, a 100-base-pair (bp) sliding window compared the even and odd signal to input across the human transcriptome (Supplementary Fig. 3a), resulting in the discovery of 3,602 enriched sites. GO analysis of TINCR-interacting genes showed enrichment of differentiation-associated genes (Fig. 3a). TINCR binding is enriched in mRNAs that are downregulated following TINCR knockdown ($P = 3.97 \times 10^{-7}$). RIA-Seq results were confirmed by RNA interactome analysis and qRT–PCR (Supplementary Fig. 3b). These data are consistent with potential TINCR action by post-transcriptional differentiation gene regulation.

LncRNAs can act together with specific proteins[3,4,19–21]. To identify TINCR-binding proteins of relevance to epidermal differentiation control, we developed human protein microarray analysis (Supplementary Fig. 2d, right). *TINCR* sense and antisense RNA were transcribed with Cy5 and independently hybridized to a protein microarray containing approximately 9,400 recombinant human proteins (Human ProtoArray). STAU1 protein displayed the strongest *TINCR* RNA binding (Fig. 3b and Supplementary Fig. 3c). Reciprocal binding was confirmed by two-way ribonucleoprotein complex pull-down experiments (Fig. 3c, d). STAU1 is a known RNA-binding protein[22–24] first identified in *Drosophila* as a mediator of RNA localization in oocytes[25]; however, a role for STAU1 in epidermal differentiation has not been described. Similar to TINCR loss, STAU1 deficiency phenocopied impaired differentiation of epidermal tissue (Fig. 4a and Supplementary Fig. 3d). Transcript profiling of STAU1-deficient epidermis showed significant overlap of STAU1- and TINCR-regulated genes (42.5% overlap for siSTAU1 (short interfering RNA (siRNA) against *STAU1*), 47.8% for siTINCR, $P = 1.24 \times 10^{-222}$) (Fig. 4b, Supplementary Fig. 3e and Supplementary Table 4). Gene set enrichment analysis (GSEA)[26] of siSTAU1 as well as siTINCR gene sets showed marked overlap with the keratinocyte differentiation signature published previously[7] (Supplementary Fig. 3f, g) indicating that TINCR together with STAU1 is required for epidermal differentiation.

To study TINCR interaction with differentiation mRNAs, the top 1,500 TINCR enriched sites detected by RIA-Seq were subjected to a *de novo* motif search. This identified a 25-nucleotide motif that was strongly enriched in TINCR-interacting mRNAs and also repeated within TINCR itself, termed the TINCR box (Fig. 4c, Supplementary Fig. 4 and Supplementary Table 5). A reverse search for the TINCR box in all TINCR-enriched sites using the find individual motifs occurrences (FIMO) algorithm yielded sequence similarity ($P < 10 \times 10^{-4}$) for 96.3% of the 3,602 sites present. By contrast, a reverse search of the TINCR box in the least TINCR-enriched sites showed sequence similarity ($P < 1 \times 10^{-4}$) for 11.3% of analysed 2,567 sites, indicating strong enrichment of the TINCR box motif in TINCR-interacting mRNAs. To investigate whether the TINCR box is also relevant for interaction with TINCR- and STAU1-regulated mRNAs, TINCR-binding transcripts were overlapped with those showing differential expression in TINCR- and STAU1-deficient epidermis. Reverse motif search with enriched sequences of the resulting 31 genes (Supplementary Fig. 5a) also showed high occurrence of the TINCR box (Fig. 4c). Of note, 3 out of those 31 mRNAs were previously shown to interact with STAU1 protein in a

kidney cell line[27]. Analysis of TINCR secondary structure in solution by selective hydroxyl acylation analyzed by primer extension (SHAPE)[28] showed that TINCR boxes of three, six, seven and ten reside in open RNA structure conformations (Supplementary Fig. 6a, b) that may be amenable to TINCR-target interactions. By contrast, analysis of microRNA (miRNA) seed sequences showed no enrichment for any miRNA seed in mRNAs affected by TINCR knockdown, arguing against a competing endogenous RNA (ceRNA) mechanism for TINCR (Supplementary Tables 6 and 7). STAU1 depletion did not affect TINCR subcellular localization (Supplementary Fig. 5e). To test whether the TINCR motif is required for target mRNA binding to TINCR, pull-down experiments were performed with a wild-type and TINCR-box-deficient target mRNA. Full TINCR binding to the *PGLYRP3* differentiation gene mRNA occurred with or without STAU1 protein, but was dependent on the 3′ *PGLYRP3* TINCR box (Fig. 4d, e). However, the existence of TINCR- and STAU1-regulated differentiation gene mRNAs that don't show direct interaction with TINCR (Supplementary Table 8) suggests the potential existence of other mechanisms of indirect target regulation in this setting.

Recent work showed that STAU1-binding sites could be created by imperfect base pairing between an ALU element of an mRNA target of STAU1-mediated decay (SMD) and another ALU sequence in a half-STAU1-binding site lncRNA; STAU1 binding to this sequence leads to mRNA degradation in a UPF1/2-dependent manner[23]. The lack of change in TINCR transcript levels in STAU1-depleted epidermis (Supplementary Fig. 5b) and the direct binding of TINCR to STAU1 without other RNAs (Fig. 3b–d and Supplementary Fig. 3c) indicate that TINCR is neither a direct degradation target of STAU1 nor a half-STAU1-binding site RNA. Moreover, a reverse search found that only 142 of the 3,602 enriched TINCR target sites contain an ALU element, 28 of which showed enrichment for the TINCR motif ($P < 10 \times 10^{-4}$), suggesting that most TINCR–mRNA interactions occur independently of ALU elements. To test whether TINCR–STAU1 acts by UPF1/2-dependent SMD, we generated UPF1-deficient as well as UPF1/2 double-deficient human epidermal tissue. UPF depletion failed to alter epidermal differentiation substantially (Supplementary Fig. 5c, d), indicating that siTINCR differentiation defects are not due to disrupting SMD and thus occur through a previously uncharacterized mechanism. To explore this, differentiation mRNA stability was assessed as a function of TINCR and STAU1 for the two TINCR box motif-containing differentiation mRNA, *KRT80*, in differentiating keratinocytes using actinomycin D. Although *KRT80* mRNA decreased by 24.6% after 2 h in control differentiating keratinocytes, in siTINCR/siSTAU1 double-deficient keratinocytes it decreased by 91.3% (Supplementary Fig. 7), consistent with differentiation mRNA stabilization by TINCR and STAU1.

Among lncRNAs regulators[3,29,30], TINCR acts in somatic differentiation post-development. TINCR may control differentiation mRNA abundance post-transcriptionally, as indicated by TINCR cytoplasmic localization, TINCR binding to differentiation mRNAs and the effect of TINCR on differentiation mRNA stability. Binding of TINCR to interacting mRNAs occurs through the TINCR box motif. Loss of the TINCR-associated cytoplasmic protein STAU1 resembles TINCR loss and demonstrates a new UPF1/2-independent role for STAU1 in differentiation.

METHODS

Tissue culture

Primary human keratinocytes were isolated from freshly discarded skin surgical samples and grown in a 1:1 mixture of KSF-M (Gibco) and Medium 154 for keratinocytes (Gibco), supplemented with epidermal growth factor and bovine pituitary extract. Cells were cultured at 37 °C in a humidified chamber with 5% CO_2. Keratinocyte differentiation was induced *in*

vitro by the addition of 1.2 mM calcium to the media, then cells were grown in full confluence for up to 8 days.

Gene transfer

All siRNA oligonucleotide duplexes used in this work were synthesized by Dharmacon. One-million primary human keratinocytes were electroporated with 1 nmol siRNA oligonucleotide, using the Amaxa human keratinocyte Nucleofector kit (Lonza) as well as Amaxa Nucleofection reagents as described previously[8]. The following siRNA oligonucleotides were used for this work: siControl (sense sequence): 5′-GUAGAUUCAUAUUGUAAGGUU-3′; siTINCRA (sense sequence): 5′-GCAUGAAGUAGCAGGUAUUUU-3′; siTINCRB (sense sequence): 5′-GAUCCCGAGUGAGUCAGAAUU-3′; siSTAU1A (target sequence): 5′-GCAGGGAGUUUGUGAUGCA-3′; siSTAU1B (target sequence): 5′-CGAGU AAAGCCUAGAAUCA-3′; siUPF1A (target sequence): 5′-CAGCGGAUCGUGU GAAGAA-3′; siUPF1B (target sequence): 5′-CAAGGUCCCUGAUAAUUAU-3′.

Organotypic human epidermal tissue

For the generation of organotypic human epidermis, primary human keratinocytes were nucleofected with siRNA oligonucleotides and cultured for 12–36 h. Four-hundred-thousand nucleofected keratinocytes were seeded onto devitalized dermis and raised to the air–liquid interface to initiate stratification and differentiation of the epidermis culture as described previously[7,8].

Immunofluorescence and tissue analysis

Seven-micrometre-thick skin sections from human organotypic skin cultures were fixed in 100% methanol or acetone for 10 min followed by blocking in PBS with 10% bovine serum albumin (BSA) for 30 min. Sections were incubated with primary antibodies for 1 h. Primary antibodies were diluted in PBS with 1% BSA and include collagen type VII (Calbiochem, 234192 for rabbit; Millipore, MAB2500 for mouse) at 1:200 dilution, filaggrin (Biomedical Technologies, BT-576) at 1:500 dilution, keratin 1 (Covance, PRB-149P) at 1:2,000 dilution, keratin 10 (Neomarkers, MS-611-P) at 1:200 dilution, loricrin (Covance, PRB-145P) at 1:200 dilution, and transglu-taminase1 (Biomedical Technology, BT-621) at 1:100 dilution. The secondary antibodies used were Alexa-555-conjugated goat anti-mouse and goat anti-rabbit IgG (Molecular Probes, 1:300 dilution), and Alexa-488-conjugated goat anti-rabbit and goat anti-mouse IgG (Molecular Probes, 1:300 dilution). The nuclear dye Hoechst 33342 (Molecular Probes) was used at 1:1,000 dilution. For histological analysis, human organotypic epidermal tissue was fixed in 10% formalin (Sigma-Aldrich), embedded in paraffin, sectioned and stained with haematoxylin and eosin.

Transmission electron microscopy

Organotypic human epidermal tissue was fixed in 2% paraformaldehyde, 2% glutaraldehyde, 0.1 M cacodylate buffer, pH 7.3, 0.06% $CaCl_2$, post-fixed with ruthenium tetroxide (Polysciences) for 45 min and stained for 15 min in 1:1 saturated uranyl acetate. After three washes in water, samples were dehydrated and infiltrated with EMbed-812 resin (EMS) mixed 1:1 with propylene oxide for 2 h followed by two parts EMbed-812 to one part propylene oxide overnight. The samples were then placed into EMbed-812 for 2–4 h, transferred into moulds with fresh resin, oriented and incubated at 65 °C overnight. Ultrathin sections (80 nm) were picked up on formvar/carbon-coated slot copper grids and examined with the JEOL JEM-1400 TEM at 80 kV. Photos were taken using a Gatan Orius digital camera.

qRT–PCR analysis

Total RNA from cells was isolated with Trizol reagent (Invitrogen) and genomic DNA removed using the TurboDNase kit (Ambion) and quantified by NanoDrop. Total RNA from organotypic skin cultures was isolated with the RNeasy Plus mini kit (Qiagen) according to the manufacturer's instructions. One-microgram of total RNA was reverse transcribed with the iScript cDNA synthesis kit (Biorad). qRT–PCR was performed using the Maxima SYBR Green qPCR master mix (2×, Fermentas) and the Stratagene Mx3000P (Agilent Technologies) thermocycler. Samples were run in triplicate and normalized to 18S rRNA, *GAPDH* or ribosomal protein L32. The following primer sequences were used: 18S forward: 5′-GCAATTATTCCCCATGAACG-3′, reverse: 5′-GG CCTCACTAAACCATCCAA-3′; L32 forward: 5′-AGGCATTGACAACAGG GTTC-3′, reverse: 5′-GTTGCACATCAGCAGCACTT-3′; *GAPDH* forward: 5′-GAAGAGAGAGACCCTCACTGCTG-3′, reverse: 5′-ACTGTGAGGAGGGG AGATTCAGT-3′; *FLG* forward: 5′-AAAGAGCTGAAGGAACTTCTGG-3′, reverse: 5′-AACCATATCTGGGTCATCTGG-3′; *KRT1* forward: 5′-TGAGCTG AATCGTGTGATCC-3′, reverse: 5′-CCAGGTCATTCAGCTTGTTC-3′; *KRT10* forward: 5′-GCAAATTGAGAGCCTGACTG-3′, reverse: 5′-CAGTGGACACA TTTCGAAGG-3′; *LOR* forward: 5′-CTCTGTCTGCGGCTACTCTG-3′, reverse: 5′-CACGAGGTCTGAGTGACCTG-3′; *STAU1* forward: 5′-ATGGTATCGGCAAGGATGTG-3′, reverse: 5′-AGACATTGGTCCGTTTCCTG-3′; *ALOX12B* forward: 5′-AGACTGCAATTCCGGATCAC-3′, reverse: 5′-TGTGGAATGCA CTGGAGAAG-3′; *ALOXE3* forward: 5′-GAGCAAAAATCTCGCCAGTC-3′, reverse: 5′-GGGCTTTGTCTCAGAAATCG-3′; *ABCA12* forward: 5′-AACAG TCCAAAGCCATCCAG-3′, reverse: 5′-GAGCAGCAGCAATTTCACAG-3′; *CASP14* forward: 5′-TTCCGAAGAAGACCTGGATG-3′, reverse: 5′-TGG GGTCTCTTTTCATGGTG-3′; *ELOVL3* forward: 5′-TTCGAGGAGTATTG GGCAAC-3′, reverse: 5′-GAAGATTGCAAGGCAGAAGG-3′; *TINCR* forward: 5′-TGTGGCCCAAACTCAGGGATACAT-3′, reverse: 5′-AGATGACAGTGGC TGGAGTTGTCA-3′; *ANCR* forward: 5′-GCCACTATGTAGCGGGTTTC-3′, reverse: 5′-ACCTGCGCTAAGAACTGAGG-3′; *LINC1* forward: 5′-TTCTGGA TGCAGCCACACTTCACA-3′, reverse: 5′-TGCCAGAGGAATTCTGTTTT-3′; *UPF1* forward: 5′-ATATGCCTGCGGTACAAAGG-3′, reverse: 5′-AGCTCAAT GGCGATCTCATC-3′; *HIST1H2BG* forward: 5′-ACAAGCGCTCGACCATTA CCT-3′, reverse: 5′-TGGTGACAGCCTTGGTACCTTC-3′; *PGLYRP3* forward: 5′-GCCAGGCAGTCTCATTTACC-3′, reverse: 5′-AGAGAAGCCAGCATCACCTC-3′; *PRSS27* forward: 5′-AGTTCATGCCCGTCTCAAAG-3′, reverse: 5′-GC CCTTCACCAATTACATCCT-3′.

Northern blot analysis

Total RNA from keratinocytes was isolated with Trizol reagent (Invitrogen). A TINCR-specific, radioactive DNA probe with a length of 581 bp was generated using [α-^{32}P]dCTP (Perkin Elmer) and the Megaprime DNA labelling system (GE Healthcare). Hybridization was performed using QuickHyb (Agilent), following the manufacturer's instructions.

Single–molecule RNA FISH

Keratinocytes were grown on chambered cover glasses (Lab-Tek) and fixed in 3.7% glutaraldehyde in PBS. Forty fluorophore-linked antisense DNA probes targeting the *TINCR* full-length sequence were designed using the online designer at http://www.singlemoleculefish.com. Probes mapping to homologous or repeat sequences were excluded. *In situ* hybridization and imaging was performed as described previously[17].

Full transcriptome RNA sequencing

RNA sequencing libraries were prepared with the mRNA Seq sample prep kit (Illumina), following the manufacturer's instructions. In brief, total RNA was isolated from differentiated (days 3 and 6) and progenitor human keratinocyte populations, and mRNA was extracted by polyA selection from 1–2 μg total RNA per sample. PolyA-selected RNA was fragmented and randomly primed for reverse transcription, followed by second-strand complementary DNA synthesis, end repair, adenylation of 3′ ends, adaptor ligation and PCR amplification of approximately 300-bp cDNA fragments. High-throughput full transcriptome sequencing was undertaken using the Illumina paired-end HiSeq platform with a read length of 101 nucleotides. Reads were aligned to the human reference sequence NCBI Build 36.1/hg18 with the TopHat algorithm[31], resulting in between 100 million and 110 million mapped reads per sample. Differential expression analysis was performed with Cuffdiff, using human RefSeq transcripts as a reference transcriptome. Annotated RefSeq non-coding RNAs expressed during calcium-induced differentiation at an FPKM >5 in at least one time point were selected based on greater than twofold change with false discovery rate (FDR)-adjusted $P < 0.05$ and included in the cluster heat map. Non-coding RNAs that overlapped with protein-coding genes were excluded.

Gene expression profiling

Microarray analysis was performed on biological duplicate samples. Labelling of cDNA derived from control and TINCR-depleted human organotypic epidermis was done using the MessageAmp III RNA amplification kit (Ambion), following the manufacturer's instructions. Hybridization to Affymetrix GeneChip HG-U133 Plus 2.0 arrays was carried out at Stanford's Protein and Nucleic Acid Facility. Gene expression analysis was performed as described previously[7].

RNA interactome analysis

Antisense DNA probes were designed targeting the *TINCR* full-length sequence using the online designer at http://www.singlemoleculefish.com. Probes mapping to homologous or repeat sequences were excluded. Thirty-eight probes were generated and split into two sets based on their relative positions along the TINCR sequence such that even-numbered and odd-numbered probes were separately pooled, similar in design to other RNA-binding approaches taken successfully in single-molecule RNA FISH[17]. All probes were biotinylated at the 3′ end with an 18-carbon spacer arm (Protein and Nucleic Acid Facility, Stanford University). Cells were grown in differentiation conditions and rinsed once with room-temperature PBS, followed by fixation with 1% glutaraldehyde in PBS for 10 min at room temperature. Crosslinking was then quenched with 0.125 M glycine for 5 min. Cells were rinsed again with PBS, scraped into Falcon tubes, and pelleted at 1,500*g*. Cell pellets were snap frozen in liquid nitrogen and could be stored at −80 °C. To prepare lysates, cell pellets were quickly thawed in a 37 °C water bath and resuspended in cell lysis buffer (50 mM Tris, pH 7.0, 10 mM EDTA, 1% SDS, and added just before use: dithithreitol (DTT), phenyl-methylsulphonyl fluoride (PMSF), protease inhibitor and Superase-In) at 100 mg ml^{-1} on ice for 10 min, and sonicated using Bioruptor (Diagenode) until lysates were completely solubilized. RNA was in the size range of 100 to 500 nucleotides. Cell lysate was diluted in double the volume of hybridization buffer (500 mM NaCl, 1% SDS, 100 mM Tris, pH 7.0, 10 mM EDTA, 15% formamide, and added just before use: DTT, PMSF, protease inhibitor, and Superase-In. Probes (100 pmol) were added to 3 ml of diluted lysate, which was mixed by end-to-end rotation at 37 °C overnight. Streptavidin-magnetic C1 beads were washed three times in cell lysis buffer, 1 mg (100 μl) of beads was added to hybridization reaction per 100 pmol of probes, and the whole reaction was mixed for 30 min at 37 °C. Beads–biotin-probes–RNA adducts were captured by magnets (Invitrogen) and washed five times with a wash buffer volume equivalent to ten times the volume of the

beads (2×SSC, 0.5% SDS, fresh PMSF added). After the last wash, buffer was removed carefully. For RNA elution, beads were resuspended in 200 μl RNA proteinase K buffer (100 mM NaCl, 10 mM Tris, pH 7.0, 1 mM EDTA, 0.5% SDS) and 1 mg ml^{-1} proteinase K (Ambion). After incubation at 50 °C for 45 min, followed by boiling for 10 min, RNA was isolated using Trizol reagent. Eluted RNA was subject to DNase treatment (TURBO DNase kit, Ambion) followed by qRT–PCR for the detection of enriched transcripts. For TINCR box removal, full-length *PGLYRP3* (1,077-bp length) was cut with the restriction endonuclease CspCI, resulting in loss of a 96-bp fragment at the 3′ end of the transcript. *LacZ* RNA was added as control. qRT–PCR data was normalized to *TINCR* and *LacZ*. For high-throughput sequencing, RNA was first converted into cDNA using the Ovation V2 kit (Nugen). cDNA samples were then fragmented to an average of 130 bp by Covaris sonicator, and 200 ng of shortened cDNA samples was converted into libraries compatible with Illumina Genome Analyzer IIx using the NEBNext ChIP-seq Library prep set (NEB). Approximately 22 million to 32 million reads were mapped per sample and used for downstream analysis.

RIA-Seq data analysis

Sequencing reads were mapped to NCBI build 36.1/hg18 using TopHat[31] with default options. Search for enriched peaks in the ‘even’ and ‘odd’ samples compared to input control was performed by scanning each gene using 100-nucleotide sliding windows. The number of reads overlapping with each sliding window was calculated using the ‘coverageBed’ function from BEDTools for even, odd, and input samples[32]. Signals in even, odd and input samples were defined as normalized read counts to the total number of aligned reads in each sample. Only sliding windows that have at least one read in every sample were included for downstream analysis. Enrichment score of each sliding window was defined as:

$$\mathrm{EScore}_i = \frac{\min(\mathrm{even\_signal}_i, \mathrm{odd\_signal}_i)}{\mathrm{input\_signal}_i}$$

The average $\log_2$(EScore) and standard deviation of $\log_2$(EScore) were also calculated and noted here as mean and s.d. A sliding window was defined as an enriched site if its $\log_2$(EScore) > mean + 1.5 s.d. We discovered 3,602 enriched sliding windows, which cover 1,852 RefSeq genes (defined to be enriched genes). Enriched sliding windows were ranked by EScore and sequences of the top 1,500 sliding windows were extracted and used for *de novo* motif search in MEME[33]. Sequences of genes that were enriched in RIA-Seq and also differentially expressed in siTINCR and siSTAU (significance analysis of microarrays FDR < 0.05 and greater than twofold change in signal intensity in siControl versus siTINCR or siSTAU1 samples) were also extracted for reverse motif search using the FIMO algorithm[33]. GO terms associated with enriched genes were calculated using DAVID[34].

ProtoArray hybridization

The sense and antisense *TINCR* RNAs were *in vitro* transcribed from the pBluescriptR-TINCR vector (Open Biosystems) using T7 and T3 polymerases (Promega) in accordance with the manufacturer’s instructions. RNA labelling for microarray hybridizations was performed using the Label IT μArray Cy5 labelling kit (Mirus) to achieve the labelling efficiency of roughly 3 pmol Cy5 dye per microgram of RNA. Human Protein Microarrays v5.0 (Invitrogen) were independently hybridized with 10 pmol sense and antisense strands of *TINCR* RNA in 40 mM Tris-HCl, pH 8.0, 150 mM sodium chloride, 0.5 mM magnesium acetate, 10 μg ml^{-1} Yeast transfer RNA, 10 μg ml heparin, 1 mM DTT, 0.01% Igepal CA-630, 5% glycerol and 0.2 U μl^{-1} RNaseOUT (Invitrogen), incubated in the dark at 25 °C for 1 h and after extensive washes spin dried and scanned at 635 nm (Cy5) using the

GenePix 4000B Microarray scanner (Molecular Devices). The intensity of the 635-nm signal at each spotted protein location was determined with GenePix Pro 6.1 software (Molecular Devices). To quantify RNA–protein interactions, the intensity of the 635-nm signal (F635) was divided by the local background intensity (B635) at each of the duplicate spots for a given protein. Data were filtered based on signal above background, including duplicate features with mean signal intensities greater than twofold above local background into the analysis. For the visualization process, the array images from antisense RNA hybridizations were pseudocoloured green and overlaid with the sense RNA hybridization images.

Protein immunoprecipitation with subsequent RNA detection

For *in vitro* protein–RNA complex immunoprecipitation, pcDNA3.1Hygro-STAU1-HA plasmid containing carboxy terminal 3×HA-tagged human staufen1 was *in vitro* translated using the rabbit reticulocyte lysate system (Promega) according to the manufacturer's instructions. The sense strands of full-length human non-coding RNAs (*TINCR*, *LINC1* and *ANCR*) were *in vitro* transcribed using T7 promoter. Two-hundred-and-fifty nanograms of *TINCR*, *LINC1* (325 nucleotides; chr1q21.3) or *ANCR* (855 nucelotides; chr4q12) RNA were combined with 12.5 μl *in vitro* translated STAU1–HA in immunoprecipitation buffer containing 40 mM Tris-HCl, pH 8.0, 150 mM sodium chloride, 0.5 mM magnesium acetate, 20 g ml^{-1} μ heparin, 1 mM DTT, 0.01% or 1% Igepal CA-630, 5% glycerol, 0.2 U μl^{-1} RNaseOUT (Invitrogen) and protease inhibitor Complete Mini (Roche). After 1 h of incubation STAU1–HA was immunoprecipitated with 20 μl Protein G Dynabeads (Invitrogen), bound to 2.5 μg anti-HA antibody (HA.11, clone 16B12, Covance), washed extensively with immunoprecipitation buffer, and RNA from the residual mixture was extracted with phenol–chloroform followed by ethanol precipitation. The cDNA was then synthesized with iScript cDNA synthesis kit (Bio-Rad) and subjected to qRT–PCR.

In vitro RNA pull-down with subsequent protein detection

For *in vitro* RNA pull-down, *TINCR*, *LacZ* and *ANCR* mRNAs were labelled with biotin-16-UTP (GE Healthcare) during *in vitro* transcription reaction according to the manufacturer's instructions. Five microlitres of *in vitro* translated STAU1–HA was incubated with 1 μg biotin–16-UTP-labelled *TINCR*, *LacZ* or *ANCR* in immunoprecipitation buffer for 30 min at 25 °C. After addition of 5 μl of MyOne Streptavidin T1 Dynabeads (Invitrogen), the mixture was incubated for a further 30 min and subjected to five wash cycles of 5 min, each using 500 μl IPB buffer. After the final wash, magnetic beads were resuspended in 12 μl protein-loading buffer, RNA-bound protein separated by SDS–PAGE and detected with anti-HA monoclonal antibody (Covance, MMS-101P) by western blot analysis. Western blot analysis was performed as described previously[8].

RNA stability assay

For analysis of RNA stability, keratinocytes were treated with actinomycin D (6 μg ml^{-1}) at day 3 of differentiation. Cells were collected at 0, 4, 12 and 20 h time points and RNA extracted using Trizol reagent (Invitrogen). Reverse transcription was performed using oligo(dT) primers and mRNA levels were measured by qRT–PCR.

Characterization of TINCR motif box secondary structure

For the acylation of TINCR in a typical *in vitro* modification protocol, 6 μg total RNA was heated in metal-free water for 2 min at 95 °C. The RNA was then flash-cooled on ice. The RNA 3× SHAPE buffer (333 mM HEPES, pH 8.0, 20 mM magnesium chloride, 333 mM sodium chloride) was added and the RNA was allowed to equilibrate at 37 °C for 10 min. To

this mixture, 1 μl of 10×electrophile (130 mM, NMIA) stock, with or without dimethylsulphoxide, was added. The reaction was permitted to continue until the desired time. Reactions were extracted once with acid phenol–chloroform (pH 4.5 ± 0.2) and twice with chloroform. RNA was precipitated with 40 μl of 3 M sodium acetate buffer, pH 5.2, and 1 μl of glycogen (20 $\mu g\ \mu l^{-1}$). Pellets were washed twice with 70% ethanol and resuspended in 10 μl RNase-free water. For reverse transcription of modified RNA, [^{32}P]-end-labelled DNA primers were annealed to 3 μg of total RNA by incubating at 95 °C for 2 min followed by a step-down cooling (2 °C s^{-1}) to 4 °C. To the reaction first-strand buffer, DTT and deoxynucleotides were added. The reaction was preincubated at 52 °C for 1 min, then superscript III (2 U μl^{-1} final concentration) was added. Extensions were performed for 10 min. To the reaction, 1 μl of 4 M sodium hydroxide was added and allowed to react for 5 min. Ten microlitres of gel loading buffer II (Ambion) was then added and cDNA extensions were resolved on 8% denaturing (7 M urea) polyacrylamide gels (29:1 acrylamide:bisacrylamide, 1% TBE).

For the characterization of reverse transcription stops, cDNA extensions were visualized by phosphorimaging (STORM, Molecular Dynamics). cDNA bands were integrated with SAFA[35]. SHAPE reactivities were normalized to a scale spanning 0 to 1.5, in which 1.0 is defined as the mean intensity of highly reactive nucleotides[36]. RNA secondary structures were predicted using mFOLD software[37]. For secondary structure analysis, the following TINCR radiolabelled RT primers were used: (1) 5′-CCTTGATGTGGTAGCGCTTCCAGCGC-3′; (2) 5′-AGACA GGGCACCCAGGGCCCCAAGAGG-3′; (3) 5′-TGTCCTGGGCAAGAGCGGAAGTGCCTC-3′; (4) 5′-AAAGCAGCTCCAGCAGGTCTGCCTGCCG-3′; (5) 5′-GGGCACACAGTGGGTCTCTGGGGACAAAG-3′; (6) 5′-TACTGTTTGTTAAATGTCAAAACACCCTG-3′; (7) 5′-TTTCCTCGGTGTGGCTGTGGGACCTTAGG-3′; (8) 5′-AAGCCTATCAGGCCTGGAGCTTCCTCAAAG-3′; (9) 5′-GAAGTAGCAGGTATTGAAGCTAGG-3′; and (10) 5′-TGCTGGGAGGAGA CACAGACCTCC-3′.

Supplementary Material

Refer to Web version on PubMed Central for supplementary material.

Acknowledgments

This work was supported by US Veterans Affairs Office of Research and Development funding to P.A.K. and National Institutes of Health (National Institute of Arthritis and Musculoskeletal and Skin Diseases) grant AR49737 to P.A.K., and by NIH R01-HG004361 and California Institute for Regenerative Medicine to H.Y.C. H.Y.C. is an Early Career Scientist of the Howard Hughes Medical Institute.

References

1. Guttman M, et al. Chromatin signature reveals over a thousand highly conserved large non-coding RNAs in mammals. Nature. 2009; 458:223–227. [PubMed: 19182780]
2. Khalil AM, et al. Many human large intergenic noncoding RNAs associate with chromatin-modifying complexes and affect gene expression. Proc Natl Acad Sci USA. 2009; 106:11667–11672. [PubMed: 19571010]
3. Rinn JL, et al. Functional demarcation of active and silent chromatin domains in human *HOX* loci by noncoding RNAs. Cell. 2007; 129:1311–1323. [PubMed: 17604720]

4. Martianov I, Ramadass A, Serra Barros A, Chow N, Akoulitchev A. Repression of the human dihydrofolate reductase gene by a non-coding interfering transcript. Nature. 2007; 445:666–670. [PubMed: 17237763]
5. Pauli A, Rinn JL, Schier AF. Non-coding RNAs as regulators of embryogenesis. Nature Rev Genet. 2011; 12:136–149. [PubMed: 21245830]
6. Wan D, et al. Large-scale cDNA transfection screening for genes related to cancer development and progression. Proc Natl Acad Sci USA. 2004; 101:15724–15729. [PubMed: 15498874]
7. Sen GL, Reuter JA, Webster DE, Zhu L, Khavari PA. DNMT1 maintains progenitor function in self-renewing somatic tissue. Nature. 2010; 463:563–567. [PubMed: 20081831]
8. Truong AB, Kretz M, Ridky TW, Kimmel R, Khavari P. A p63 regulates proliferation and differentiation of developmentally mature keratinocytes. Genes Dev. 2006; 20:3185–3197. [PubMed: 17114587]
9. O'Driscoll J, et al. A recurrent mutation in the loricrin gene underlies the ichthyotic variant of Vohwinkel syndrome. Clin Exp Dermatol. 2002; 27:243–246. [PubMed: 12072018]
10. Smith FJ, et al. Loss-of-function mutations in the gene encoding filaggrin cause ichthyosis vulgaris. Nature Genet. 2006; 38:337–342. [PubMed: 16444271]
11. Virtanen M, Smith SK, Gedde-Dahl T Jr, Vahlquist A, Bowden PE. Splice site and deletion mutations in keratin (*KRT1* and *KRT10*) genes: unusual phenotypic alterations in Scandinavian patients with epidermolytic hyperkeratosis. J Invest Dermatol. 2003; 121:1013–1020. [PubMed: 14708600]
12. Elias PM. Stratum corneum defensive functions: an integrated view. J Invest Dermatol. 2005; 125:183–200. [PubMed: 16098026]
13. Eckl KM, et al. Molecular analysis of 250 patients with autosomal recessive congenital ichthyosis: evidence for mutation hotspots in *ALOXE3* and allelic heterogeneity in *ALOX12B*. J Invest Dermatol. 2009; 129:1421–1428. [PubMed: 19131948]
14. Sakai K, et al. *ABCA12* is a major causative gene for non-bullous congenital ichthyosiform erythroderma. J Invest Dermatol. 2009; 129:2306–2309. [PubMed: 19262603]
15. Westerberg R, et al. Role for ELOVL3 and fatty acid chain length in development of hair and skin function. J Biol Chem. 2004; 279:5621–5629. [PubMed: 14581464]
16. Denecker G, et al. Caspase-14 protects against epidermal UVB photodamage and water loss. Nature Cell Biol. 2007; 9:666–674. [PubMed: 17515931]
17. Raj A, van den Bogaard P, Rifkin SA, van Oudenaarden A, Tyagi S. Imaging individual mRNA molecules using multiple singly labeled probes. Nature Methods. 2008; 5:877–879. [PubMed: 18806792]
18. Chu C, Qu K, Zhong FL, Artandi SE, Chang HY. Genomic maps of long noncoding RNA occupancy reveal principles of RNA-chromatin interactions. Mol Cell. 2011; 44:667–678. [PubMed: 21963238]
19. Huarte M, et al. A large intergenic noncoding RNAinduced by p53 mediates global gene repression in the p53 response. Cell. 2010; 142:409–419. [PubMed: 20673990]
20. Nagano T, et al. The *Air* noncoding RNA epigenetically silences transcription by targeting G9a to chromatin. Science. 2008; 322:1717–1720. [PubMed: 18988810]
21. Tsai MC, et al. Long noncoding RNA as modular scaffold of histone modification complexes. Science. 2010; 329:689–693. [PubMed: 20616235]
22. Dugré-Brisson S, et al. Interaction of Staufen1 with the 5′ end of mRNA facilitates translation of these RNAs. Nucleic Acids Res. 2005; 33:4797–4812. [PubMed: 16126845]
23. Gong C, Maquat LE. lncRNAs transactivate STAU1-mediated mRNA decay by duplexing with 3′ UTRs via Alu elements. Nature. 2011; 470:284–288. [PubMed: 21307942]
24. Kiebler MA, et al. The mammalian staufen protein localizes to the somatodendritic domain of cultured hippocampal neurons: implications for its involvement in mRNA transport. J Neurosci. 1999; 19:288–297. [PubMed: 9870958]
25. St Johnston D, Beuchle D, Nusslein-Volhard C. Staufen, a gene required to localize maternal RNAs in the *Drosophila* egg. Cell. 1991; 66:51–63. [PubMed: 1712672]

26. Subramanian A, et al. Gene set enrichment analysis: a knowledge-based approach for interpreting genome-wide expression profiles. Proc Natl Acad Sci USA. 2005; 102:15545–15550. [PubMed: 16199517]
27. Furic L, Maher-Laporte M, DesGroseillers L. A genome-wide approach identifies distinct but overlapping subsets of cellular mRNAs associated with Staufen1- and Staufen2-containing ribonucleoprotein complexes. RNA. 2008; 14:324–335. [PubMed: 18094122]
28. Merino EJ, Wilkinson KA, Coughlan JL, Weeks KM. RNA structure analysis at single nucleotide resolution by selective 2′-hydroxyl acylation and primer extension (SHAPE). J Am Chem Soc. 2005; 127:4223–4231. [PubMed: 15783204]
29. Bond AM, et al. Balanced gene regulation by an embryonic brain ncRNA is critical for adult hippocampal GABA circuitry. Nature Neurosci. 2009; 12:1020–1027. [PubMed: 19620975]
30. Young TL, Matsuda T, Cepko CL. The noncoding RNA *Taurine Upregulated Gene 1* is required for differentiation of the murine retina. Curr Biol. 2005; 15:501–512. [PubMed: 15797018]
31. Trapnell C, Pachter L, Salzberg SL. TopHat: discovering splice junctions with RNA-Seq. Bioinformatics. 2009; 25:1105–1111. [PubMed: 19289445]
32. Quinlan AR, Hall IM. BEDTools: a flexible suite of utilities for comparing genomic features. Bioinformatics. 2010; 26:841–842. [PubMed: 20110278]
33. Bailey TL, et al. MEME SUITE: tools for motif discovery and searching. Nucleic Acids Res. 2009; 37:W202–W208. [PubMed: 19458158]
34. Huang DW, Sherman BT, Lempicki RA. Systematic and integrative analysis of large gene lists using DAVID bioinformatics resources. Nature Protocols. 2009; 4:44–57.
35. Das R, Laederach A, Pearlman SM, Herschlag D, Altman RB. SAFA: semi-automated footprinting analysis software for high-throughput quantification of nucleic acid footprinting experiments. RNA. 2005; 11:344–354. [PubMed: 15701734]
36. Deigan KE, Li TW, Mathews DH, Weeks KM. Accurate SHAPE-directed RNA structure determination. Proc Natl Acad Sci USA. 2009; 106:97–102. [PubMed: 19109441]
37. Zuker M. Mfold web server for nucleic acid folding and hybridization prediction. Nucleic Acids Res. 2003; 31:3406–3415. [PubMed: 12824337]

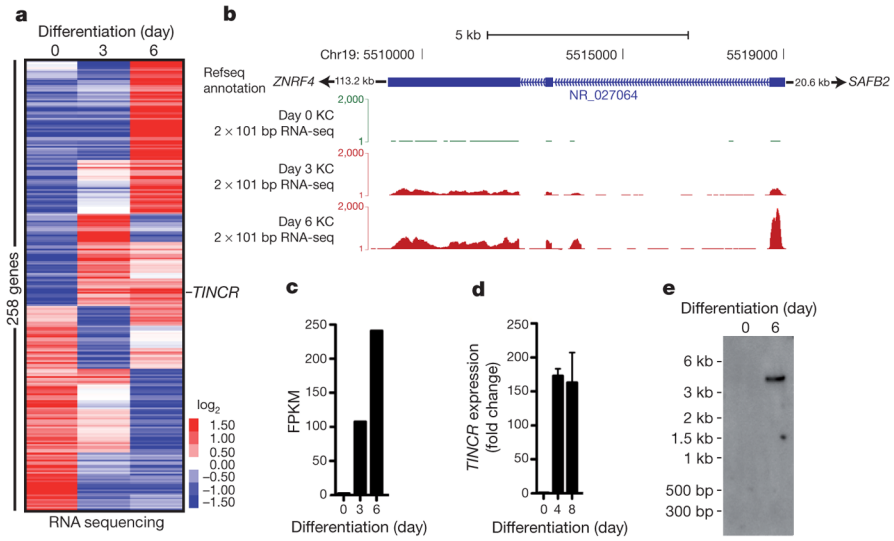

Figure 1. TINCR is induced during epidermal differentiation

a, Mean-centred, hierarchical clustering of 258 annotated non-coding RNAs altered (>twofold change) in undifferentiated cells (day 0) and during days of calcium-induced differentiation *in vitro*. **b**, Schematic of *TINCR* genomic locus on chromosome 19. Day 0, 3 and 6 of keratinocyte (KC) differentiation; blue rectangles represent exons. **c**, Relative TINCR abundance in fragments per kilobase of exon model per million mapped fragments (FPKM). **d**, *TINCR* qRT–PCR. Error bars are s.d., $n = 4$. **e**, Northern blot analysis, with TINCR the single band seen in differentiation; bp, base pairs.

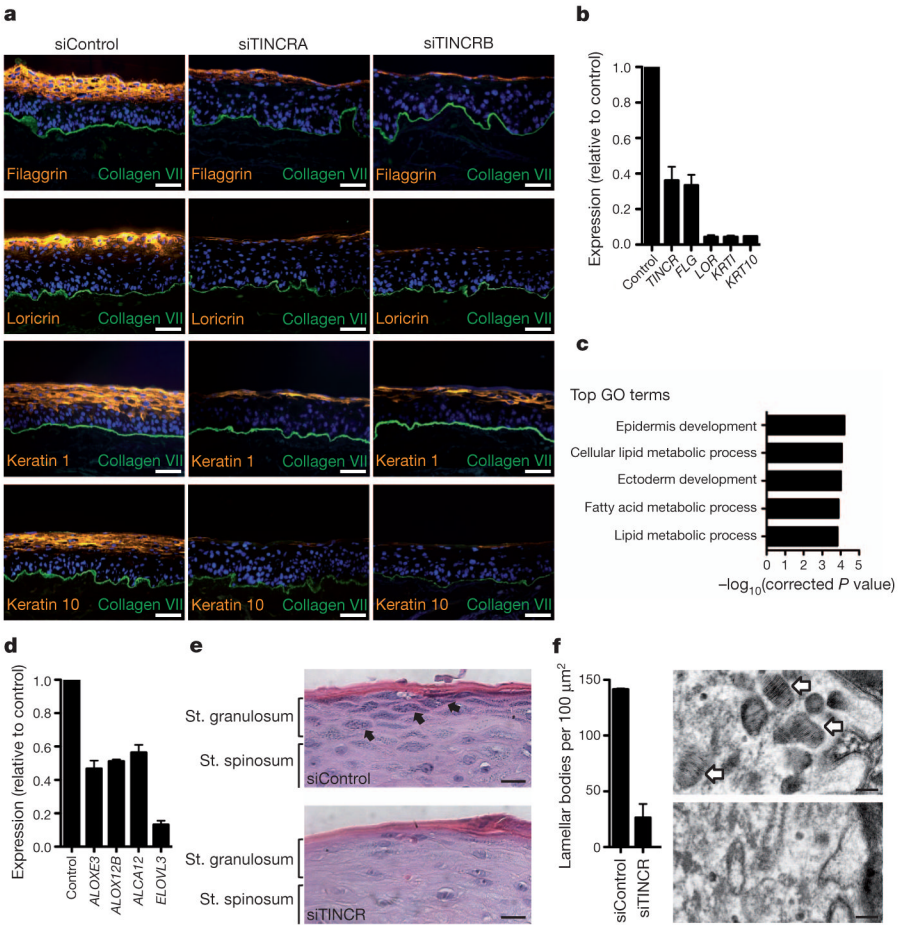

Figure 2. TINCR regulates epidermal differentiation genes involved in barrier formation

a, Loss of differentiation proteins in TINCR-depleted organotypic human epidermis by independent *TINCR* siRNAs (siTINCRA and siTINCRB) versus scrambled control (siControl); nuclei stained blue (Hoechst 33342). Scale bars, 50 μm. **b**, mRNA expression in TINCR-deficient tissue versus control; duplicate biological replicates for duplicate independent TINCR siRNAs. Error bars are s.d., $n = 6$. **c**, GO terms significantly enriched in the TINCR-depleted gene subset. **d**, mRNA expression of lipid barrier synthesis genes in TINCR-depleted tissue. Error bars denote s.d., $n = 4$. **e**, Loss of protein-rich keratohyalin granules (arrows in control) in TINCR-deficient organotypic human epidermis. St, stratum. Scale bars, 10 μm. **f**, Loss of normal lipid-containing lamellar bodies (arrows in control, top image) in TINCR-depleted tissue (bottom image) ($n = 3$). Scale bars, 100 nm.

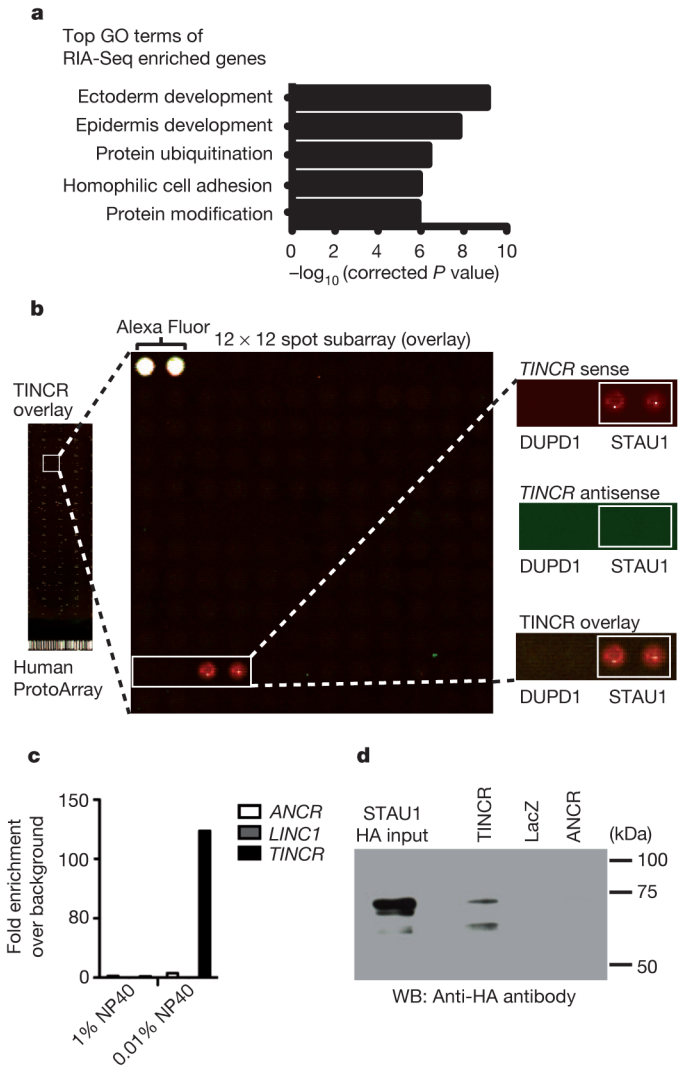

Figure 3. TINCR interacts with differentiation mRNAs and STAU1 protein

a, Enriched GO terms in TINCR-interacting genes detected by RIA-Seq. **b**, Protein microarray analysis detects *TINCR* RNA binding to STAU1 protein. Human recombinant protein microarray spotted with approximately 9,400 proteins (left); enlarged 144 protein spot subarray (middle) demonstrating strand-specific binding of TINCR sense strand to STAU1 protein (right); DUPD1 protein negative control is shown. Alexa-Fluor-647-labelled rabbit anti-mouse IgG in the top left corner of each subarray. **c**, STAU1 protein immunoprecipitation pulls down *TINCR* RNA. *ANCR* and *LINC1* (also known as *XIST*) represent lncRNA controls. **d**, Streptavidin precipitation of *in vitro* synthesized biotinylated *TINCR* RNA pulls down STAU1 protein. HA, haemagglutinin; WB, western blot.

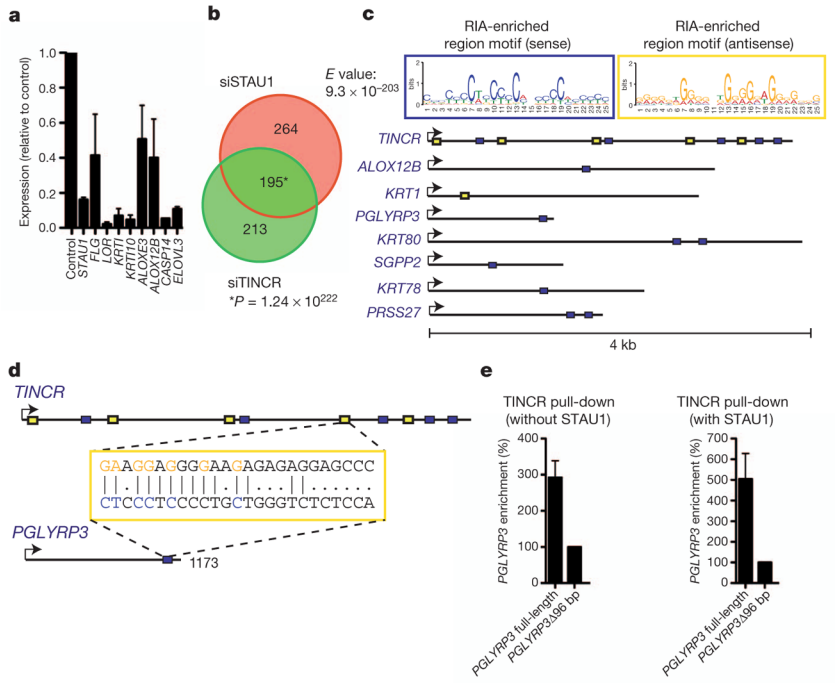

Figure 4. Differentiation regulation by *TINCR* RNA and STAU1 protein

a, Diminished expression of TINCR-regulated genes in STAU1-depleted organotypic tissue in independent biological replicates for duplicate independent STAU1 siRNA treatments. Error bars are s.d., $n = 3$. **b**, Overlap of 672 genes regulated by TINCR and STAU1 **c**, Location of the TINCR box motif in *TINCR* as well as selected *TINCR*-associated differentiation mRNAs. RIA, RNA interactome analysis. **d**, TINCR motif base-pairing between the *TINCR* transcript and *PGLYRP3* differentiation gene mRNA. **e**, Biotinylated *TINCR* RNA with or without STAU1 protein pulls down the full-length 1,077-bp *PGLYRP3* mRNA at higher efficiency than TINCR box-depleted *PGLYRP3* (*PGLYRP3*Δ96 bp). Error bars denote s.d. and are too small to be visible for the *PGLYRP3*Δ96 samples; $n = 3$.